Pergamon

Int. J. Heat Mass Transfer. Vol. 39, No. 7, pp. 1439–1452, 1996

0017-9310/96 $15.00+0.00

0017-9310(95)00189-1

Transient natural convection heat transfer between concentric and vertically eccentric spheres

CHENG PING CHIU and WEN RUEY CHEN

Department of Mechanical Engineering, National Cheng Kung University, Tainan, Taiwan, Republic of China

(*Received* 4 *November* 1994 *and in final form* 23 *March* 1995)

Abstract—Transient analysis has been investigated numerically to determine heat transfer by natural convection between concentric and vertically eccentric spheres with isothermal boundary conditions. The inner and outer spheres were heated and cooled in a step change of temperature. The governing equations, in terms of vorticity, stream function and temperature were expressed in a radial coordinate transformation coordinate system. The alternating direction implicit method and the successive over-relaxation techniques were applied to solve the finite difference form of governing equations. A physical model was introduced, which accounts for the effects of fluid buoyancy as well as eccentricity of the outer sphere. Transient solutions of the entire flow field were obtained for a range of Rayleigh numbers ($10^3 < Ra < 10^5$), for a Prandtl number of 0.7 and a radius ratio of 2.0, with the outer sphere near the top and bottom of the inner sphere ($\varepsilon = \pm 0.625$). Results of the parametric study conducted further reveal that the heat and flow fields are primarily dependent on the Rayleigh number and on the eccentricity of the annulus. Comparisons are attempted between the present computations and the results available in those of previous experimental and numerical studies.

INTRODUCTION

The problem of natural convection heat transfer in the annulus between two concentric and eccentric spheres has received considerable attention from researchers in many diverse fields of applications, such problems commonly occur within the geophysical fields, solar energy collectors, thermal storage systems as well as nuclear reactor design, and many other practical situations. As a result, extensive experimental and theoretical works dealing with flow and associated heat transfer characteristics of natural convection in annuli between two isothermal concentric spheres have been reported in the literature. Comprehensive reviews [1–10] on natural convection in such configuration are available, and there is no need to repeat them. However, most of the studies are concerned with the steady-state aspect of the problem, thus knowledge about transient thermal convection between two spheres is limited. A proper understanding of transient phenomena is essential to the design and operation of various engineering applications of thermal fluid systems, such as gyroscopes and energy systems including nuclear reactors. This would be the reason for the fact that studies on natural convection between concentric spheres have increased recently [11–16], Fujii *et al.* [11] obtained a numerical solution of transient laminar free convection between two concentric spheres at Prandtl number of 0.7 and Rayleigh number of 100. Later, they extended the problem for large Prandtl number, $Pr = 0.7$–100 [12]. Ozoe *et al.* [13] solved the three-dimensional analysis of natural convection in a spherical annulus between two concentric spheres, under nonsymetrical thermal boundary conditions, for $Ra = 500$ and $Pr = 1.0$. Ozoe *et al.* [14] and Mochimaru [15] presented transient natural convection in a spherical/hemispherical enclosure after a step change in the wall temperature experimentally and numerically. Chu and Lee [16] computed a numerical solution for transient natural convection between concentric spheres of various radius ratio with a large range of Rayleigh number $Ra = 10^3$–5×10^5; little attention has been paid to natural convection in eccentric spheres of engineering interest.

The present paper is motivated by interest in demonstrating the effects of eccentricity as well as buoyancy in the transient natural convection flow between two vertical eccentric spheres. A finite difference solution is obtained for the governing equations in terms of stream function, vorticity and temperature in a spherical polar coordinate system. The effect of eccentricity and Rayleigh number on the fluid flow and heat transfer characteristics are discussed. It may be noted that for concentric spheres ($\varepsilon = 0$), the governing equations in the present paper can be deduced to the equations reported by Chu and Lee [16]. The details of the method are described in the next section. We wish to point out that our formulation is more general for various natural convection problems involving concentric and vertically eccentric spheres.

NOMENCLATURE

C_p	specific heat at constant pressure
e	vertical eccentricity
g	local gravitational acceleration
h	heat transfer coefficient
k	thermal conductivity
L	annular gap, $\bar{r}_o - \bar{r}_i$
Nu	local Nusselt number, hL/k
$\overline{Nu}$	average Nusselt number, hL/k
P	dimensionless gauge pressure, $(\bar{P}-\bar{P}_o)L^2/\rho\alpha^2$
$\bar{P}$	absolute pressure
$\bar{P}_o$	surrounding pressure
Pr	Prandtl number, v/α
r	dimensionless coordinate, $\bar{r}/L$
$\bar{r}$	radial coordinate
R	dimensionless radial profile of outer sphere, $\bar{R}/L$
$\bar{R}$	radial profile of outer sphere
Ra	Rayleigh number, $(g\beta\Delta\bar{T}L^3)/(v\alpha)$
R^*	ratio of outer and inner radius ratio, r_o/r_i
t	time
T	dimensionless temperature, $(\bar{T}-\bar{T}_o)/(\bar{T}_i-\bar{T}_o)$
$\bar{T}$	temperature
v	velocity
V	dimensionless velocity, vL/α.

Greek symbols

α	thermal diffusivity
β	thermal expansion coefficient
$\Delta\bar{T}$	temperature difference between spheres, $\bar{T}_i-\bar{T}_o$
ε	dimensionless vertical eccentricity, e/L
η	radial coordinate in transformed plane, $(r-r_i)/(r_o-r_i)$
θ	dimensionless angular coordinate, $\bar{\theta}/\pi$
$\bar{\theta}$	angular coordinate
θ^*	angular position at vortex center
v	kinematic viscosity
ρ	fluid density
τ	dimensionless time, $t\alpha/L^2$
ψ	dimensionless stream function, $\bar{\psi}/\alpha L$
$\bar{\psi}$	stream function in spherical coordinates
ω	dimensionless vorticity, $\bar{\omega}L^2/\alpha$
$\bar{\omega}$	vorticity.

Subscripts

i, o	inner and outer
max	maximum
min	minimum.

MATHEMATIC FORMULATION

The geometric configuration of the physical system is a concentric or vertically eccentric arrangement of two circular spheres of radii r_o and r_i located at O' and O, respectively. The eccentricity of the outer sphere is measured by the distance ε. If the outer sphere is placed above the central position, ε has a positive value, otherwise ε is negative. For a natural convective heat transfer problem, the largest heat transfer variation due to eccentricity occurs when the direction of ε is aligned with the gravitational direction. Therefore, this study focuses on the problem that ε is vertically shifted.

The space between the inner and outer spheres is filled by the viscous and incompressible Newtonian fluid. Initially, the annulus is at a uniform temperature T_o and a quiescent state is assumed, while the temperature of the inner sphere is suddenly changed to a higher temperature T_i and the outer sphere is maintained at T_o. To formulate the problem, it is assumed that: (1) the flow within the annulus is laminar; (2) all fluid properties, are taken to be constant, except for the density variation with temperature in the buoyancy term, i.e. the Boussinesq approximation is valid; (3) the flow is symmetrical about vertical axis parallel to the line of gravity acceleration even produces the multi-cellular flow, furthermore; (4) viscous dissipation and radiation effect can be neglected.

A spherical polar coordinate system (r, θ, φ) was chosen as shown in Fig. 1. To deal with the numerical formulation associated with the complex physical domain of the vertical eccentric annulus, a radial coordinate transformation is adopted to map the eccentric annular gap into a unit sphere. The outer sphere radius $r = R(\theta)$ is transformed into the unit sphere $\eta = 1$, while the inner sphere radius $r = r_i$ is transformed into the pole $\eta = 0$ [17].

This transformation is obtained by defining a new

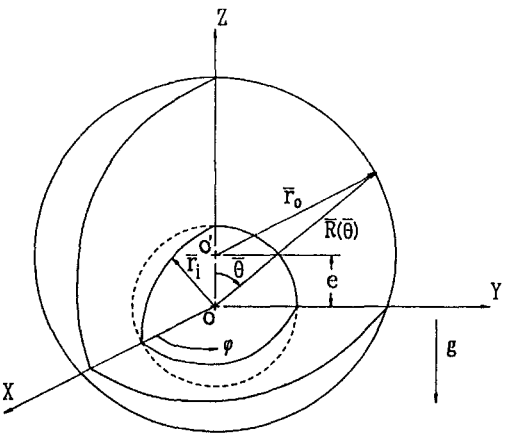

Fig. 1. Coordinate system for the spherical annulus.

radial coordinate as

$$\eta = \frac{r - r_i}{R(\theta) - r_i}. \tag{1}$$

Where $R(\theta)$ denotes variable dimensionless profile of the outer sphere measured from the center of the inner sphere, which is symmetric with respect to the vertical axis in any angular position of φ-direction and is expressed by

$$R(\theta) = \sqrt{r_o^2 - \varepsilon^2 \sin\theta} + \varepsilon \cos\theta. \tag{2}$$

The governing equations for the two-dimensional problem fluid in the dimensionless term can be written as

Vorticity transport equation

$$\frac{\partial \omega}{\partial \tau} + \frac{1}{\pi r^2 \sin(\pi\theta)} \left\{ \left(\frac{\partial \eta}{\partial r}\right)\left[\frac{\partial \psi}{\partial \eta}\frac{\partial \omega}{\partial \theta} - \frac{\partial \psi}{\partial \theta}\frac{\partial \omega}{\partial \eta}\right] + \left[\left(\frac{1}{r}\frac{\partial \eta}{\partial \theta} - \pi \cot(\pi\theta)\frac{\partial \eta}{\partial r}\right)\frac{\partial \psi}{\partial \eta} + \frac{1}{r}\frac{\partial \psi}{\partial \theta}\right]\omega \right\}$$
$$= Pr\left[\nabla_1^2 - \frac{1}{r^2 \sin^2(\pi\theta)}\right]\omega + Pr \cdot Ra\left[\left(\sin(\pi\theta)\frac{\partial \eta}{\partial r} + \frac{\cos(\pi\theta)}{\pi r}\frac{\partial \eta}{\partial \theta}\right)\frac{\partial T}{\partial \eta} + \frac{\cos(\pi\theta)}{\pi r}\frac{\partial T}{\partial \theta}\right]. \tag{3}$$

Stream function equation

$$D_1^2 \psi = \omega r \sin(\pi\theta). \tag{4}$$

Energy equation

$$\frac{\partial T}{\partial \tau} + \frac{1}{\pi r^2 \sin(\pi\theta)}\frac{\partial \eta}{\partial r}\left(\frac{\partial \psi}{\partial \eta}\frac{\partial T}{\partial \theta} - \frac{\partial \psi}{\partial \theta}\frac{\partial T}{\partial \eta}\right) = \nabla_1^2 T. \tag{5}$$

Pressure equation

$$-\nabla_1^2 P = \left(\frac{\partial \eta}{\partial r}\right)^2\left(\frac{\partial V_r}{\partial \eta}\right)^2 + \frac{1}{\pi^2 r^2}\left(\frac{\partial V_\theta}{\partial \theta}\right)^2 + \frac{2}{\pi^2 r^2}\left(\frac{\partial \eta}{\partial \theta}\right)\left(\frac{\partial V_\theta}{\partial \theta}\right)\left(\frac{\partial V_\theta}{\partial \eta}\right) + \frac{1}{\pi^2 r^2}\left(\frac{\partial \eta}{\partial \theta}\right)^2\left(\frac{\partial V_\theta}{\partial \eta}\right)^2 + \frac{2}{\pi r}\left(\frac{\partial \eta}{\partial r}\right)\left(\frac{\partial V_\theta}{\partial \eta}\right)\left(\frac{\partial V_r}{\partial \theta}\right) + \frac{2}{\pi r}\left(\frac{\partial \eta}{\partial r}\right)\left(\frac{\partial \eta}{\partial \theta}\right)\left(\frac{\partial V_\theta}{\partial \eta}\right)\left(\frac{\partial V_r}{\partial \eta}\right) + \frac{2V_r}{\pi r^2}\left(\frac{\partial V_\theta}{\partial \theta}\right) + \frac{2V_r}{\pi r^2}\left(\frac{\partial \eta}{\partial \theta}\right)\left(\frac{\partial V_\theta}{\partial \eta}\right) - \frac{2V_\theta}{r}\left(\frac{\partial \eta}{\partial r}\right)\left(\frac{\partial V_\theta}{\partial \eta}\right) + \frac{2V_r^2}{r^2} + \frac{2\cot(\pi\theta)}{r^2}V_r V_\theta + \frac{\cot^2(\pi\theta)}{r^2}V_\theta^2 - Pr \cdot Ra\left\{\left[\frac{\sin(\pi\theta)}{\pi r}\left(\frac{\partial \eta}{\partial r}\right) - \cos(\pi\theta)\left(\frac{\partial \eta}{\partial \theta}\right)\right]\frac{\partial T}{\partial \eta} + \frac{\sin(\pi\theta)}{\pi r}\frac{\partial T}{\partial \theta}\right\} \tag{6}$$

where

$$\frac{\partial \eta}{\partial r} = \frac{1}{R - r_i} \tag{7}$$

$$\frac{\partial \eta}{\partial \theta} = \frac{-\eta}{R - r_i}\frac{\partial R}{\partial \theta} \tag{8}$$

$$\frac{\partial^2 \eta}{\partial \theta^2} = \frac{-1}{R - r_i}\left(\eta \frac{\partial^2 R}{\partial \theta^2} + 2\frac{\partial \eta}{\partial \theta}\frac{\partial R}{\partial \theta}\right) \tag{9}$$

$$\nabla_1^2 = \left[\left(\frac{\partial \eta}{\partial r}\right)^2 + \frac{1}{\pi^2 r^2}\left(\frac{\partial \eta}{\partial \theta}\right)^2\right]\frac{\partial^2}{\partial \eta^2} + \left[\frac{2}{\pi^2 r^2}\left(\frac{\partial \eta}{\partial \theta}\right)\right]\frac{\partial^2}{\partial \eta\, \partial \theta} + \left[\frac{1}{\pi^2 r^2}\right]\frac{\partial^2}{\partial \theta^2} + \left[\frac{2}{r}\left(\frac{\partial \eta}{\partial r}\right) + \frac{1}{\pi^2 r^2}\left(\frac{\partial^2 \eta}{\partial \theta^2}\right) + \frac{\cot(\pi\theta)}{\pi r^2}\left(\frac{\partial \eta}{\partial \theta}\right)\right]\frac{\partial}{\partial \eta} + \left[\frac{\cot(\pi\theta)}{\pi r^2}\right]\frac{\partial}{\partial \theta} \tag{10}$$

$$D_1^2 = \left[\left(\frac{\partial \eta}{\partial r}\right)^2 + \frac{1}{\pi^2 r^2}\left(\frac{\partial \eta}{\partial \theta}\right)^2\right]\frac{\partial^2}{\partial \eta^2} + \left[\frac{2}{\pi^2 r^2}\left(\frac{\partial \eta}{\partial \theta}\right)\right]\frac{\partial^2}{\partial \eta\, \partial \theta} + \left[\frac{1}{\pi^2 r^2}\right]\frac{\partial^2}{\partial \theta^2} + \left[\frac{1}{\pi^2 r^2}\left(\frac{\partial^2 \eta}{\partial \theta^2}\right) - \frac{\cot(\pi\theta)}{\pi r^2}\left(\frac{\partial \eta}{\partial \theta}\right)\right]\frac{\partial}{\partial \eta} - \left[\frac{\cot(\pi\theta)}{\pi r^2}\right]\frac{\partial}{\partial \theta}. \tag{11}$$

The associated initial and boundary conditions for the problem considered are for $\tau < 0$

$$\omega = \psi = \frac{\partial \psi}{\partial \eta} = \frac{\partial \psi}{\partial \theta} = T = 0 \text{ everywhere}, \tag{12}$$

for $\tau > 0$

at $\eta = 0$

$$\psi = \frac{\partial \psi}{\partial \eta} = 0 \quad T = 1 \quad \omega = \frac{1}{r_i \sin(\pi\theta)}\left(\frac{\partial \eta}{\partial r}\right)^2 \frac{\partial^2 \psi}{\partial \eta^2}$$

$$\frac{\partial P}{\partial \eta} = -\left[Pr\left(\frac{\cot(\pi\theta)}{r}\omega + \frac{1}{r}\frac{\partial \omega}{\partial \theta}\right) + Pr \cdot Ra \cdot T\cos(\pi\theta)\right] \quad (13)$$

at $\eta = 1$

$$\psi = \frac{\partial \psi}{\partial \eta} = 0 \quad T = 0$$

$$\omega = \frac{1}{r_o \sin(\pi\theta)}\left[\left(\frac{\partial \eta}{\partial r}\right)^2 + \frac{1}{\pi^2 r^2}\left(\frac{\partial \eta}{\partial \theta}\right)^2\right]\frac{\partial^2 \psi}{\partial \eta^2}$$

$$\frac{\partial P}{\partial \eta} = -Pr\left\{[\cot(\pi\theta)\cos(\delta) - \sin(\delta)]\frac{\omega}{r} + \frac{\cos(\delta)}{r}\frac{\partial \omega}{\partial \theta} + \left[\frac{\cos(\delta)}{\pi r}\frac{\partial \eta}{\partial \theta} - \sin(\delta)\frac{\partial \eta}{\partial r}\right]\frac{\partial \omega}{\partial \eta}\right\} + Pr \cdot Ra \cdot T[\cos(\pi\theta - \delta)] \quad (14)$$

where

$$\delta = \sin^{-1}\left[\frac{\varepsilon}{r_o}\sin(\pi\theta)\right] \quad (15)$$

at $\theta = 0, 1,$

$$\psi = \omega = \frac{\partial T}{\partial \theta} = \frac{\partial P}{\partial \theta} = 0. \quad (16)$$

From the above formulation, the governing parameters for the present problem are thus the Rayleigh number Ra, the Prandtl number Pr, the radius ratio R^* and the eccentricity ε.

The local and average Nusselt number at inner and outer radii are defined as

$$Nu_{i,o} = -\frac{1}{r_i r_o}\left[r^2 \frac{\partial \eta}{\partial r}\frac{\partial T}{\partial \eta}\right]_{\eta = 0,1} \quad (17)$$

$$\overline{Nu} = -\pi \int_0^1 Nu_{i,o}\left[\frac{\sin(\pi\theta)}{2}\right]d\theta. \quad (18)$$

NUMERICAL METHOD

To solve the problem, the governing equations as well as initial and boundary conditions were discretized by the finite difference method. Equations (3)–(5) were discretized with time derivative terms approximated by forward difference and the spatial derivative terms approximated by central difference. Derivatives at the boundaries were approximated by three-point forward or backward difference. The finite difference equation for the time-dependent vorticity transport and energy equations were solved by employing the alternating direction implicit (ADI) finite difference technique [18], while the finite difference equation for stream function was solved by the successive line relaxation method (SOR). To see the effect of mesh size on the numerical result, computations for a concentric annulus were carried out using four different mesh sizes, the resulting Nusselt numbers are presented in Fig. 2. The local Nusselt numbers, obtained from four different mesh sizes, are similar to each other, except the local value of outer sphere at $\theta = 0°$ is sensitive to the noding size, and the result seems to converge at 41×41. In order to solve the computation effort, the results presented in this article are all obtained by using the grid size of 41×41. Numerical test calculations were also performed for different time steps. Two different time steps depending on the geometry have been used for the calculations: 1×10^{-4} for $\varepsilon = 0.0$ and 5×10^{-5} for $\varepsilon = \pm 0.625$.

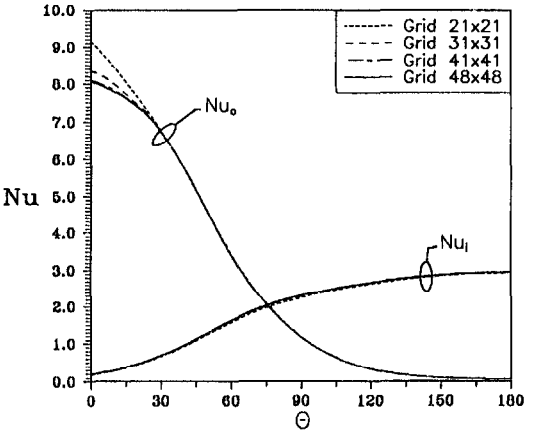

Fig. 2. Calculated local Nusselt numbers at different grid sizes ($R^* = 2.0$, $Pr = 0.7$, $Ra = 1.4 \times 10^4$).

The solution was considered convergent when the relative error between the new and old values of the field variables Φ during every time step, must be less than a prescribed criterion (10^{-4}), where Φ represents ω, ψ, T and P.

$$\frac{|\Phi_{new} - \Phi_{old}|_{max}}{|\Phi_{new}|_{max}} \leqslant 10^{-4}. \quad (19)$$

Further, the convergence of the steady-state solution was verified by checking the relative error between the present and next time step values of all field variables for inner and outer spheres within 0.1%, as shown in the following:

$$\frac{|\Phi^{n+1} - \Phi^n|_{max}}{|\Phi^{n+1}|_{max}} \leqslant 10^{-4} \quad (20)$$

where the superscripts n and $(n+1)$ indicate the nth and $(n+1)$th time step, respectively.

RESULTS AND DISCUSSION

The accuracy of the numerical solution is verified by comparing the calculated results with the measured data and other calculated results. Figure 3 shows the comparison between the calculated streamlines by the authors and the measured streamlines presented in Yin *et al.* [3]. Figure 4 shows the streamlines and isotherms in the present study and the corresponding

(a) (b)

Fig. 3. Comparison of streamlines for $R^* = 2.17$, $Pr = 0.7$ and $Ra = 7.392 \times 10^5$: (a) present results; (b) experiment results [3].

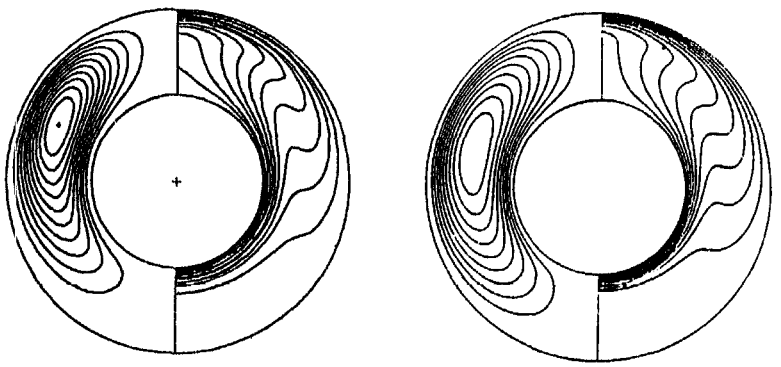

(a) (b)

Fig. 4. Comparisons of streamlines (left) and isotherms (right) for $R^* = 2.0$, $Pr = 0.7$ and $Ra = 5.0 \times 10^4$: (a) present results; (b) numerical results [7].

Table 1. Comparison of the calculated average Nusselt number $\overline{Nu}$, maximum value of stream function ψ_{max} and angular position of vortex center θ^* at steady-state, as functions of $R^* = 2.0$, $Pr = 0.7$ and $Ra = 10^3$

	Nu	ψ_{max}	θ^* (°)
Present results	1.1021	3.236	81
Mack and Hardee [4]	1.1200	3.210	77
Astill *et al.* [5]	1.1200	3.490	79
Singh and Chen [6]	1.1010	—	—
Garg [10]	1.1006	—	—
Chu and Lee [16]	1.1099	3.209	81

calculated results of Caltagirone *et al.* [7]. Table 1 compares the calculated average Nusselt number by the present study and by earlier workers [4–6, 10, 16].

Figure 5a shows a series of transient streamline and isotherm configurations for radius ratio of 2.0, Prandtl number of 0.7 and Rayleigh number of 10^4. Figure 5b presents a corresponding series of Rayleigh numbers of 10^5. This series of results is designed to

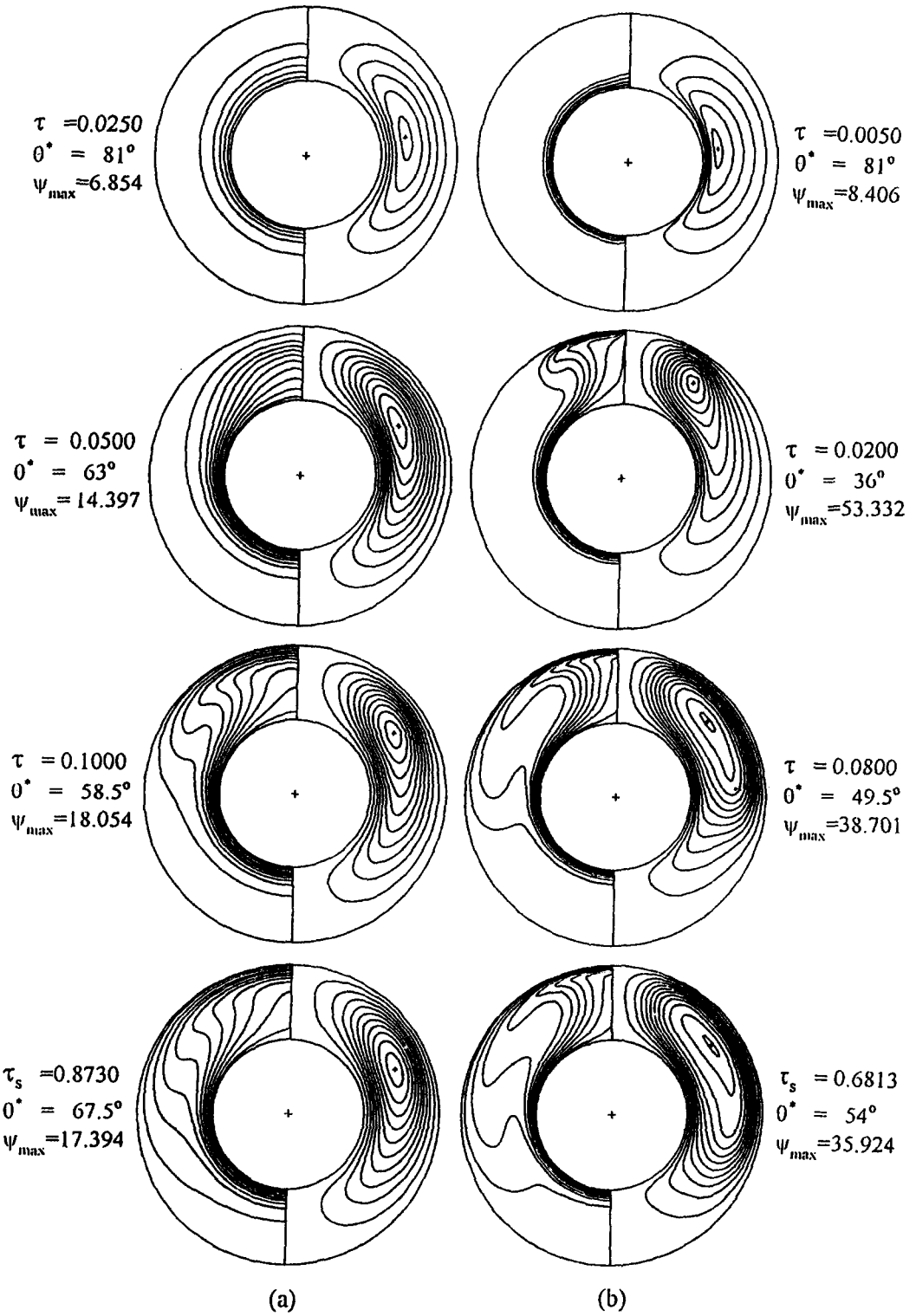

Fig. 5. Isotherms (left) and streamlines (right), for $R^* = 2.0$, $Pr = 0.7$ and $\varepsilon = 0.0$ at different time steps: (a) $Ra = 1.0 \times 10^4$; (b) $Ra = 1.0 \times 10^5$.

demonstrate the effect of Rayleigh number on the heat and fluid flow patterns in the concentric annulus. Because the problem is symmetric to the axis, each annulus contains only a half isotherm on the left and a half streamline on the right. Since the inner sphere is kept hotter, the hot fluid near the inner sphere rises upward due to thermal expansion. The uprising plume is then cooled down by the colder fluid near the upper part of outer sphere. The colder and denser fluid will eventually flow downward along the surface of the outer sphere. As time proceeds, from Fig. 5a, it is found that the position of the vortex center of the eddy first moves upward and then slowly moves downward along the annular space, while the maximum value of the stream function first increases and then slowly decreases. Until the time when steady state is reached the maximum value of the stream function $\psi_{max} = 17.394$ and the angular position of the vortex center of the crescent-shape lies at $\theta^* = 67.5°$ from the upper vertical line symmetry about midgap position. At $Ra = 10^5$, as shown in Fig. 5b, the fluid motion becomes stronger, as indicated by the increased absolute value of the stream function, and the vortex center of the eddy shifts upward. Examination of the isotherm patterns also reveals that laminar convection was the dominant mode of heat transfer, on the contrary, the pseudoconduction heat transfer regime which existed appeared in Fig. 5a. This behavior was also obtained by Bishop *et al.* [1] and Chu [16]. Next, the isotherms and streamlines for the eccentric configurations considered in this study will be examined. Figures 6 and 7 illustrate the transient streamlines and isotherms distribution at different *Ra* for positive and negative eccentricity, respectively. For positive eccentric geometry (Fig. 6) it is evident that the convective flows are both larger and stronger than for the concentric spheres. Within such a favorable configuration for convective motion, the qualitative features of streamlines and isotherms distribution depicted previously for the concentric geometry are observed to be further pronounced.

At high *Ra*, the expanse of the heat-receiving region on the outer wall is considerably extended for the positive eccentric arrangement, in contrast to the concentric spheres. On the other hand, the negative eccentric geometry provides the least favored circumstance for the development of natural convection. Both the size and strength of the fluid are markedly reduced, as shown in Fig. 7a. Moreover, Fig. 7b shows an anticlockwise rotating secondary cell in the top of the annulus as time step at $\tau = 0.08$, while the primary central eddy is clockwise. As the time step arrives at steady state, we find that a multicell flow is predicted, in which two secondary cells having a sense of rotation opposite to that of the primary central eddy are formed. One of these cells was found near the top of the inner-sphere, and the other at the bottom of the outer-sphere. These phenomena were similarly stated by Caltagirone [7], who expressed that the multicellular flows occur at a critical Rayleigh number for the radius ratio 2.0 of 5×10^4.

Figure 8 presents the influence of the Rayleigh number on the pressure distributions within the concentric annulus at different time steps. As the Rayleigh number is increased from 10^4 to 10^5, the pressure distributions are not significantly changed. With a further increase of time, it can obviously be seen from the figure that the bulk fluid, step wise-heated, produces no apparent effect on the isobars distributions. The maximum pressure is always located in the upper region of the gap.

Next, the isobars for the eccentric configurations considered in this study are also examined. Figure 9a, b illustrates the pressure distributions at different time steps and for positive and negative eccentricity, respectively. For eccentric geometries, it is evident that the pressure distributions are rather insensitive to the investigated Rayleigh number and time steps.

The transient conductive temperature distribution vs radial position, is shown in Fig. 10. The results of the steady-state analysis are compared with those of Mack and Hardee [4] and Astill *et al.* [5]. The comparison is obtained and in excellent agreement.

As a result of the difference in streamlines and isotherms, the local Nusselt number also behaved differently. Figures 11 and 12 depict the transient behavior of the local Nusselt number along the outer sphere of three geometries, considered two values of *Ra*. Examining Fig. 11b, c, and Fig. 12b, c it appears that the local Nusselt number on the outer surface has a peak near the top of the annulus at different time steps for the concentric and the positive eccentric annulus. The peak value increases with an increase in Rayleigh number. For negative eccentricity in Figs. 11a and 12a, the local Nusselt numbers on the inner and outer surface have minimum and maximum values, respectively. The generation and development with time of the maximum and minimum values will be oscillated near $\theta = 10°$–$65°$. This implies that the second flow taking place on the top of the annulus is also weak, although the Rayleigh number was increased to 10^5. This lead to the fluid at the narrow gap is an unfavorable convection motion.

Finally, the circumferentially average Nusselt numbers obtained in the present study are given in Table 2, for various Rayleigh numbers in the three annular geometries under consideration. Also included in Table 2 are the results based on the correlation for the concentric geometry reported in ref. [10], which compare favorably with the results obtained in the present study. It can be concluded that the average Nusselt number across the annulus is mainly dependent on the Rayleigh number and eccentricity. Accordingly, the present results can be correlated via a least square regression analysis in the form

$$\overline{Nu} = CRa^n \tag{21}$$

for $Pr = 0.7$ and $R^* = 2.0$, where the constant C and

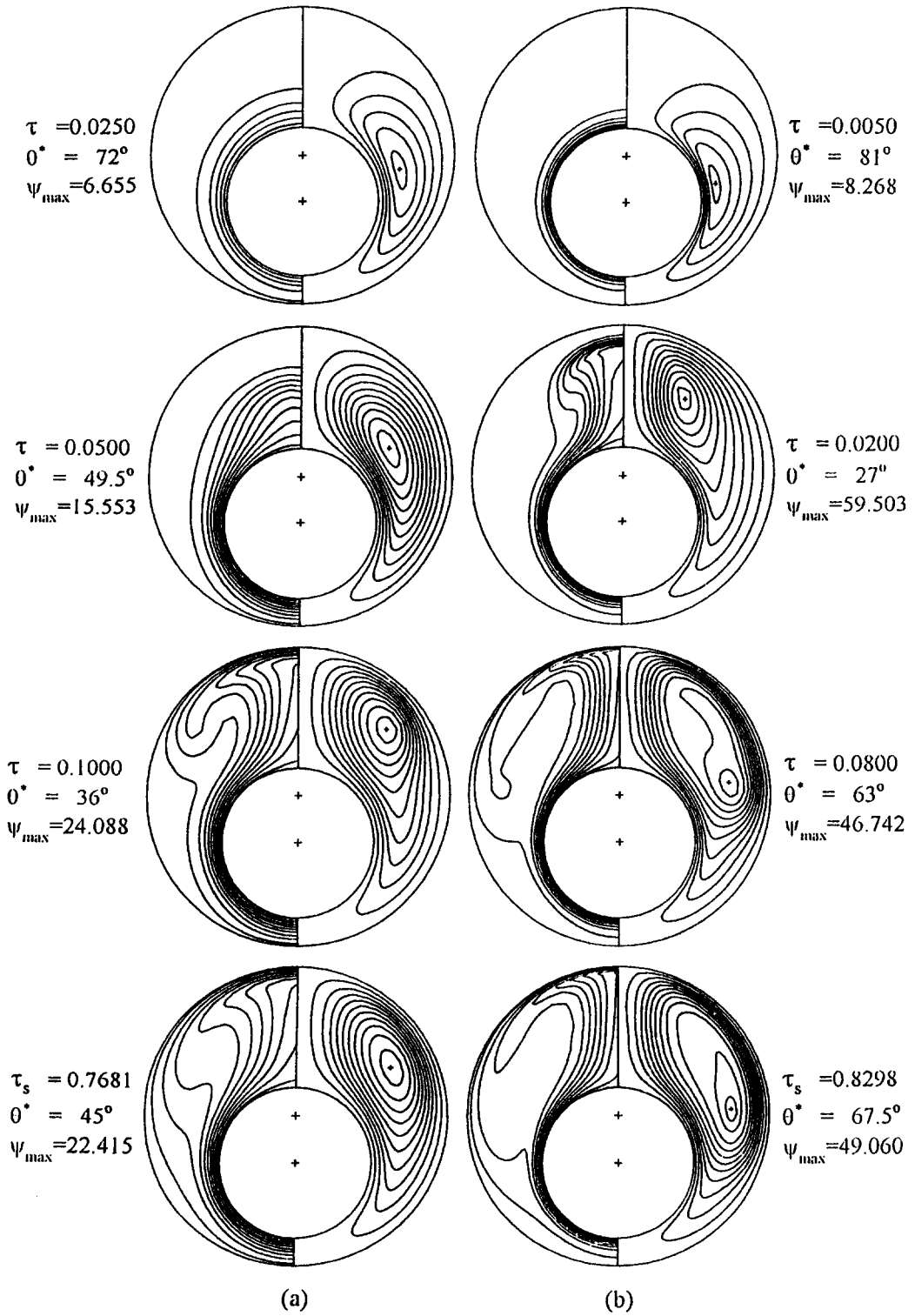

Fig. 6. Isotherms (left) and streamlines (right), for $R^* = 2.0$, $Pr = 0.7$ and $\varepsilon = 0.625$ at different time steps: (a) $Ra = 1.0 \times 10^4$; (b) $Ra = 1.0 \times 10^5$.

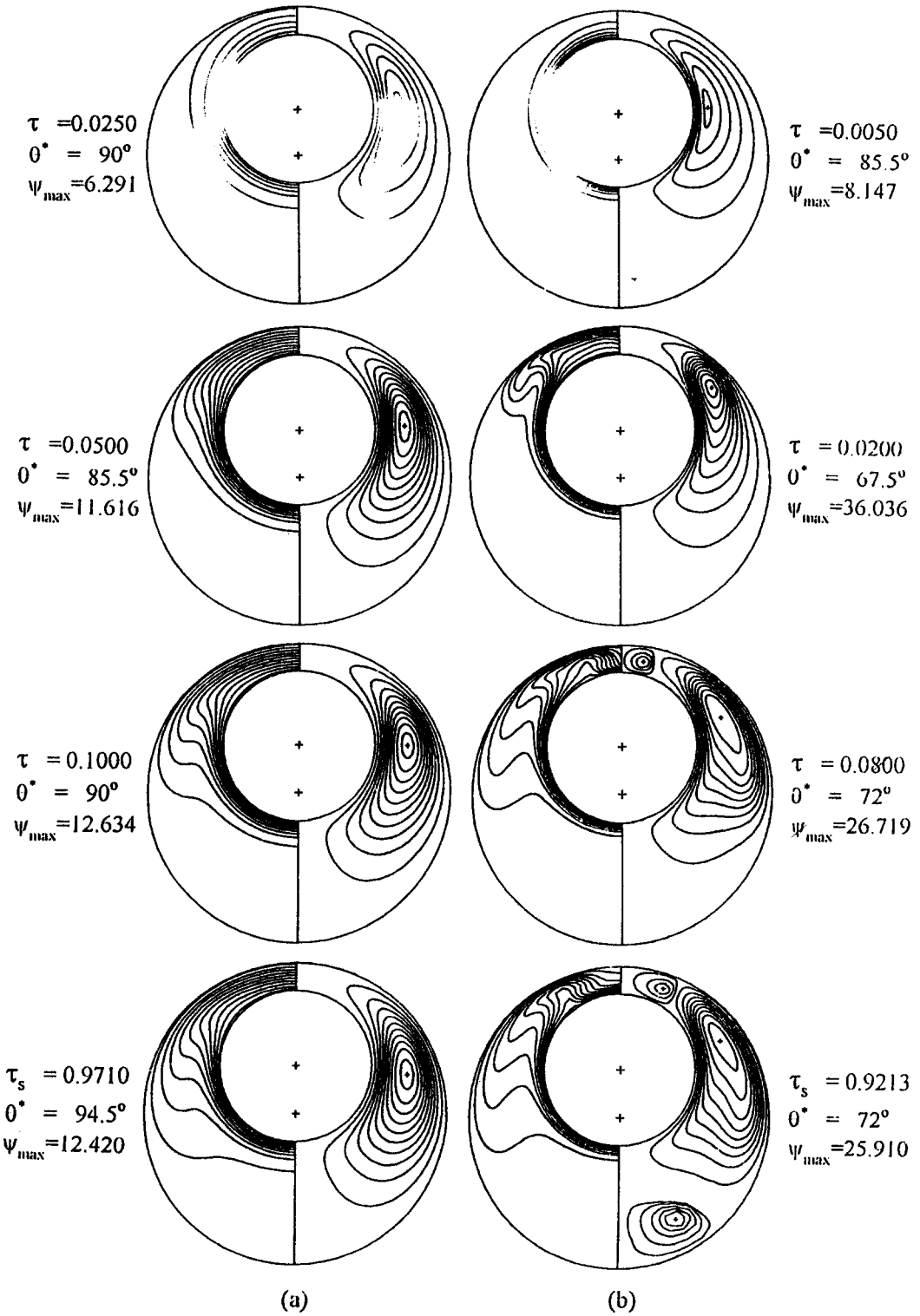

Fig. 7. Isotherms (left) and streamlines (right), for $R^* = 2.0$, $Pr = 0.7$ and $\varepsilon = -0.625$ at different time steps: (a) $Ra = 1.0 \times 10^4$; (b) $Ra = 1.0 \times 10^5$.

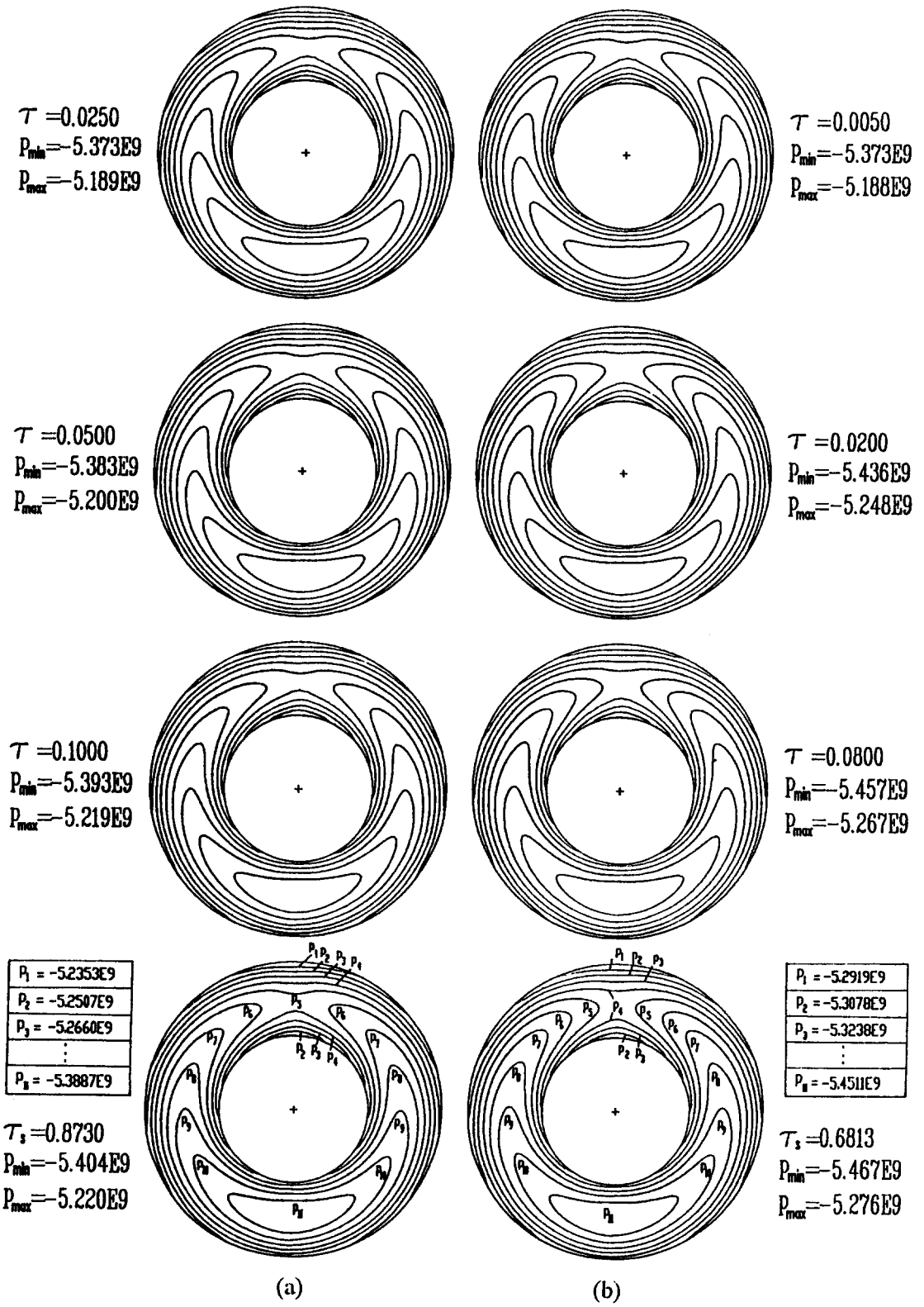

Fig. 8. Isobars for $R^* = 2.0$, $Pr = 0.7$ and $\varepsilon = 0.0$ at different time steps: (a) $Ra = 1.0 \times 10^4$; (b) $Ra = 1.0 \times 10^5$.

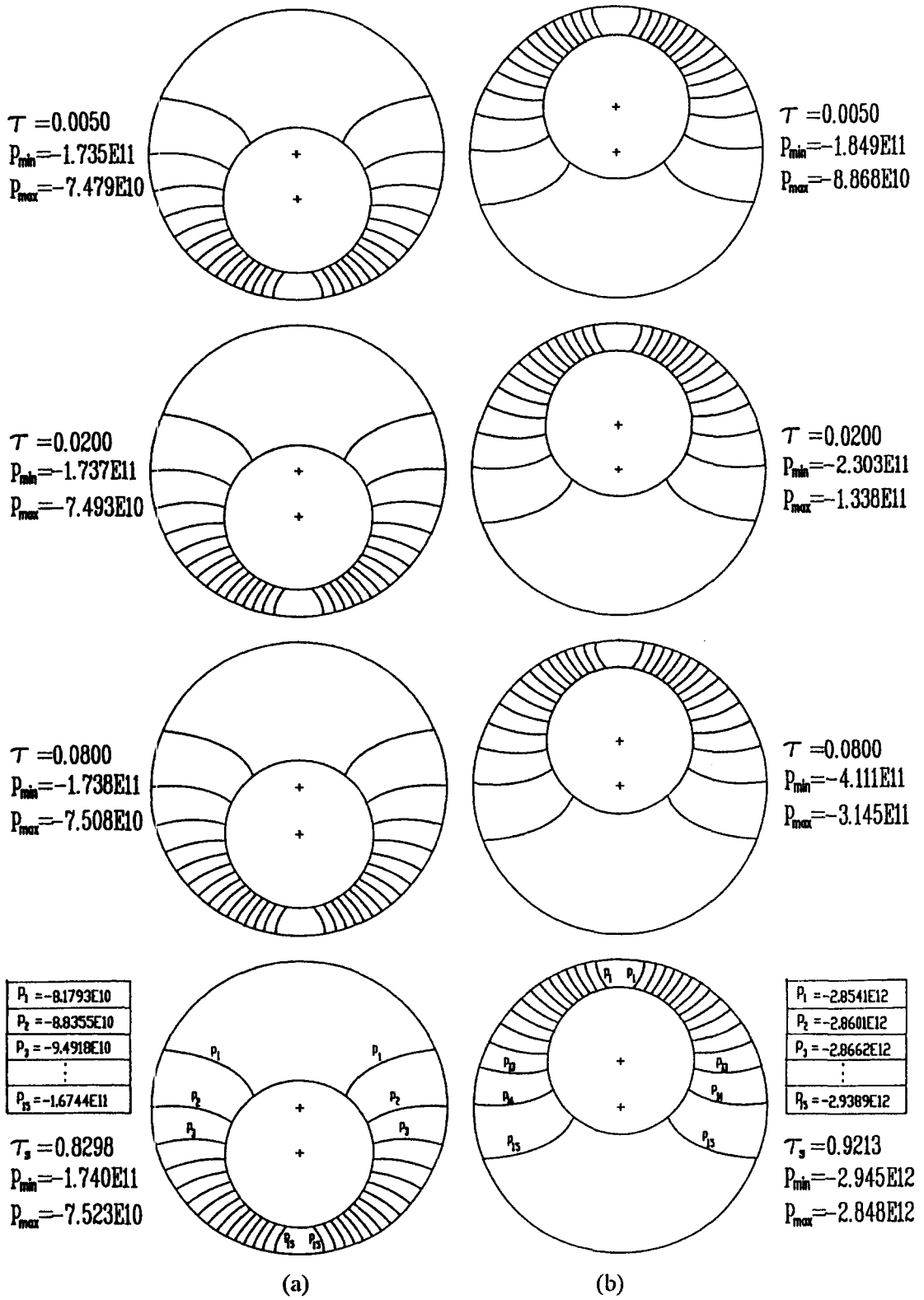

Fig. 9. Isobars for $R^* = 2.0$, $Pr = 0.7$ and $Ra = 1.0 \times 10^5$ at different time steps: (a) $\varepsilon = 0.625$; (b) $\varepsilon = -0.625$.

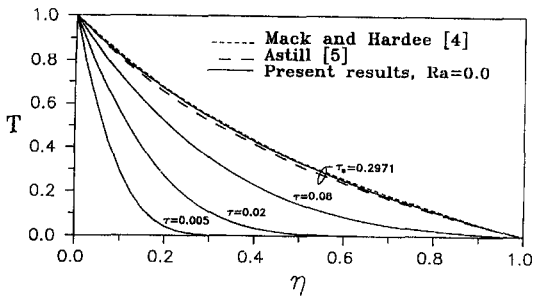

Fig. 10. Transient conduction temperature vs radial position for $R^* = 2.0$, $Pr = 0.7$ and $\varepsilon = 0.0$.

exponents m are listed in Table 3 for three configurations considered here.

In Fig. 13, the average Nusselt number is also plotted vs the Rayleigh number. The curve corresponding to $\varepsilon = 0.0$ represents the concentric case. For comparison, experimental data of Bishop *et al.* [1] and Scanlan *et al.* [2], and the numerical computation results of Chu and Lee [16] are also plotted. We observed that these results agree fairly well. Moreover, it reveals that the positive eccentricity can improve the average Nusselt number, but the negative eccentricity may not promote the conduction effect.

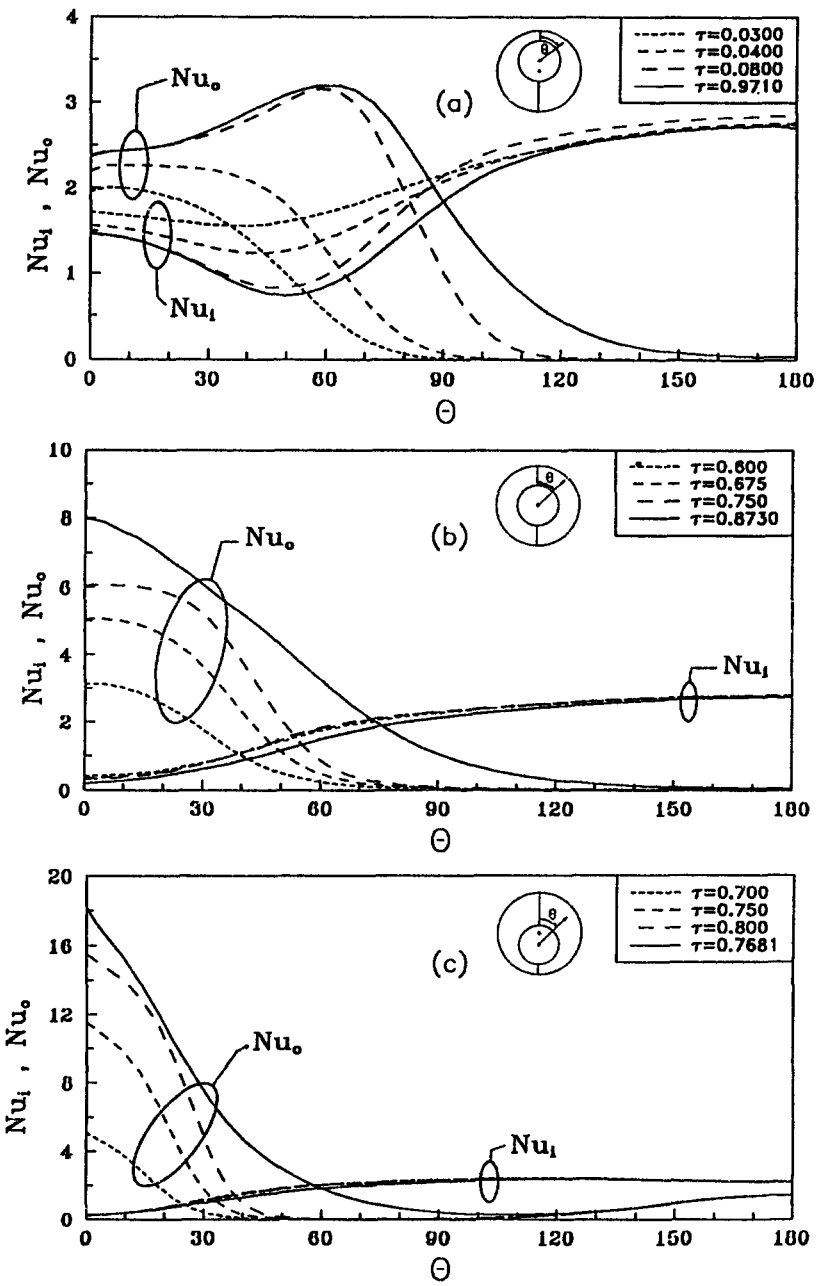

Fig. 11. Transient variation of local Nusselt numbers for $R^* = 2.0$, $Pr = 0.7$ and $Ra = 1.4 \times 10^4$: (a) $\varepsilon = -0.625$; (b) $\varepsilon = 0.0$; (c) $\varepsilon = 0.625$.

Table 2. Average Nusselt number

	$\overline{Nu}$ for Ra					
ε	10^3	5×10^3	10^4	5×10^4	10^5	5×10^5
0.625	2.4452	1.8469	1.9853	2.7567	3.3983	—
0.000	1.1021	1.7275	1.9110	2.7282	3.3555	4.8657
	(1.1006)*	(1.7393)*		(2.7761)*		
−0.625	1.1948	1.6621	1.7582	2.4703	3.1060	—

* From ref. [10].

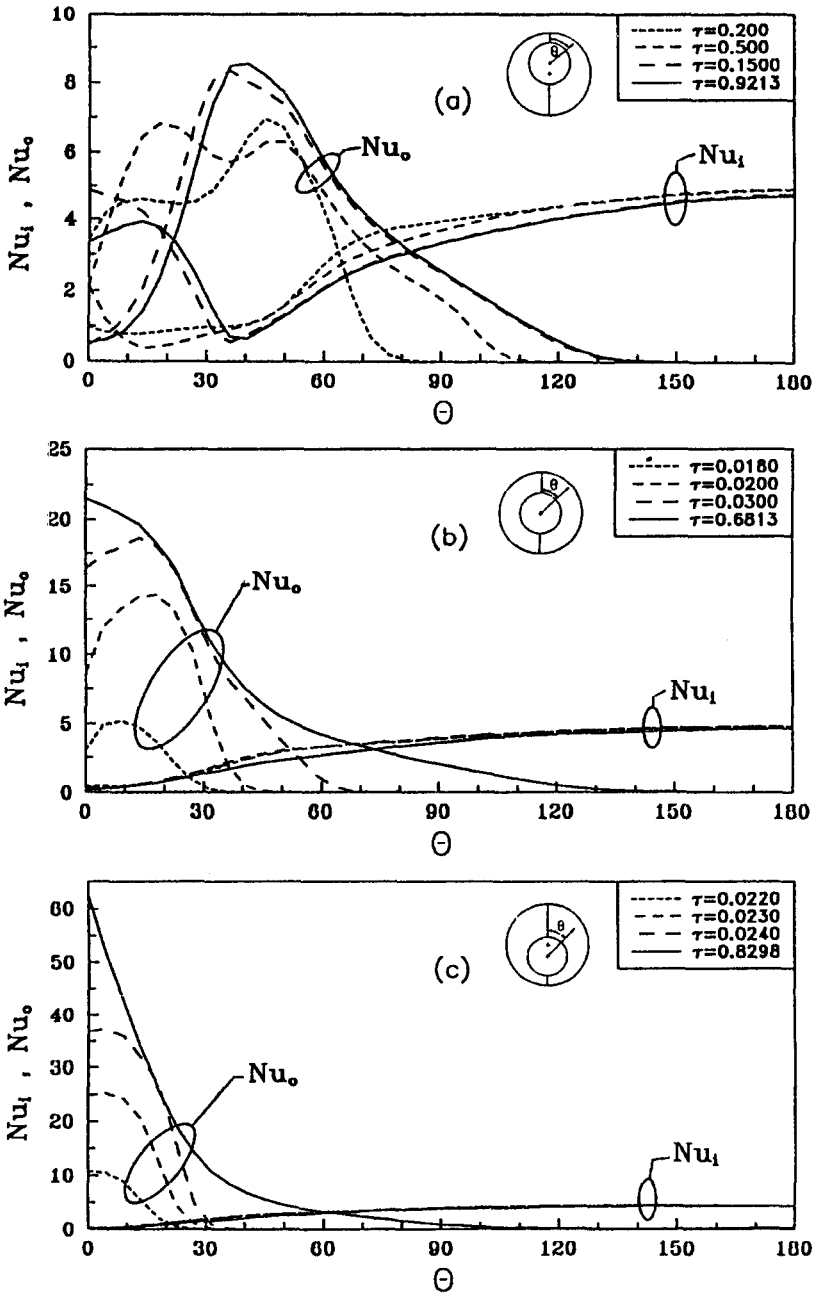

Fig. 12. Transient variation of local Nusselt numbers for $R^* = 2.0$, $Pr = 0.7$ and $Ra = 1.4\times10^5$: (a) $\varepsilon = -0.625$; (b) $\varepsilon = 0.0$; (c) $\varepsilon = 0.625$.

Table 3. Empirical constants and deviations for equation (21)

ε	C	m	Ra	Maximum deviation (%)
0.625	0.291	0.211	10^3–10^5	3.52
0.000	0.210	0.240	10^3–5×10^5	1.72
−0.625	0.267	0.209	10^3–10^5	5.33

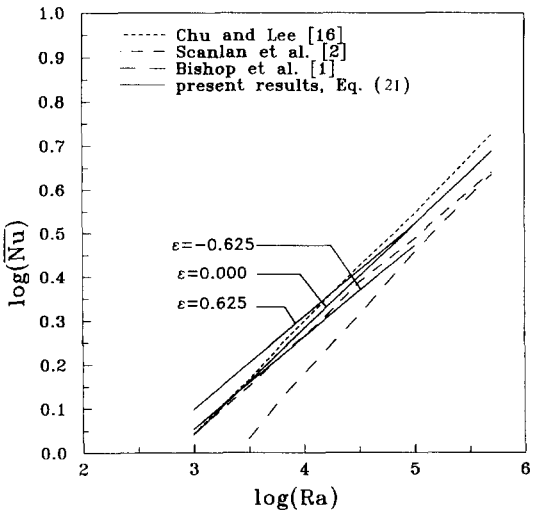

Fig. 13. Variation of Nusselt number with Raleigh number at steady state for $Pr = 0.7$ and $R^* = 2.0$.

CONCLUDING REMARKS

The transient natural convection in concentric and vertical-axially eccentric spheres with isothermal boundary conditions has been analyzed numerically by a finite difference method. The transient behaviors of the heat and fluid flows in the annuli have been vividly visualized by means of contour maps of isotherms and streamlines. The numerical results obtained further indicated that heat and fluid flow patterns in the annuli are primarily dependent on the Rayleigh number and the eccentricity. Data were plotted in the form of $\overline{Nu}$ vs Ra on a log–log plot to reveal a straight line relationship. The average Nusselt number increases with the Rayleigh number in each eccentricity displacement. The positive eccentric geometry can enhance convective heat transfer rates, but the negative eccentric geometry provides the least favored circumstance for the development of natural convection between two spheres in the annulus. A multicellular flow region begins to develop for negative eccentric geometry when $Ra = 10^5$.

Acknowledgments—Support from National Cheng Kung University for use of its computating facility is gratefully acknowledged. Also acknowledged are the referees for their useful comments.

REFERENCES

1. E. H. Bishop, L. R. Mack and J. A. Scanlan, Heat transfer by natural convection between concentric spheres, *Int. J. Heat Mass Transfer* **9,** 649–662 (1966).
2. J. A. Scanlan, E. H. Bishop and R. E. Powe, Natural convection heat transfer between concentric spheres, *Int. J. Heat Mass Transfer* **13,** 1857–1872 (1970).
3. S. H. Yin, R. E. Powe, J. A. Scanlan and E. H. Bishop, Natural convection flow patterns in spherical annuli, *Int. J. Heat Mass Transfer* **16,** 1785–1795 (1973).
4. L. R. Mack and H. C. Hardee, Natural convection between concentric spheres at low Rayleigh numbers, *Int. J. Heat Mass Transfer* **11,** 387–396 (1968).
5. K. N. Astill, H. Leong and R. Martorana, A numerical solution for natural convection in concentric spherical annuli, *Proceedings of the 19th National Heat Transfer Conference*, ASME HTD-Vol. 8, pp. 105–113 (1980).
6. S. N. Singh and J. Chen, Numerical solution for free convection between concentric spheres at moderate Grashof numbers, *Numer. Heat Transfer* **3,** 441–459 (1980).
7. J. P. Caltagirone, M. Combarnous and A. Mojtabi, Natural convection between two concentric spheres: transition toward a muticellular flow, *Numer. Heat Transfer* **3,** 107–114 (1980).
8. D. B. Ingham, Heat transfer by natural convection between spheres and cylinders, *Numer. Heat Transfer* **4,** 53–67 (1981).
9. J. L. Wright and R. W. Douglass, Natural convection in narrow-gap spherical annuli, *Int. J. Heat Mass Transfer* **29,** 725–739 (1986).
10. V. K. Garg, Natural convection between concentric spheres, *Int. J. Heat Mass Transfer* **35,** 1935–1945 (1992).
11. T. Fujii, T. Honda and M. Fujii, A numerical analysis of laminar free convection around an isothermal sphere: finite-difference solution of the full Navier–Stokes and energy equations between concentric spheres, *Numer. Heat Transfer* **7,** 103–111 (1984).
12. M. Fujii, H. Takamatsu and T. Fujii, A numerical analysis of free convection around an isothermal sphere (effects of space and Prandtl number), *Proceedings of* 1987 *ASME-JSME Thermal Engineering Joint Conference*, Vol. 4, pp. 55–60 (1987).
13. H. Ozoe, K. Fujii, T. Shibata, H. Kuriyama and S. W. Churchill, Three-dimensional numerical analysis of natural convection in a spherical annulus, *Numer. Heat Transfer* **8,** 383–406 (1985).
14. H. Ozoe, H. Kuriyama and A. Takami, Transient natural convection in a spherical and a hemispherical enclosure, *Proceedings of* 1987 *ASME-JSME Thermal Engineering Joint Conference*, Vol. 4, pp. 19–25 (1987).
15. Y. Mochimaru, Transient natural convection heat transfer in a spherical cavity, *Heat Transfer-Jap. Res.* **18,** 9–19 (1989).
16. H. S. Chu and T. S. Lee, Transient natural convection heat transfer between concentric spheres, *Int. J. Heat Mass Transfer* **36,** 3159–3170 (1993).
17. J. Prusa and L. S. Yao, Natural convection heat transfer between eccentric horizontal cylinders, *ASME J. Heat Transfer* **105,** 108–116 (1983).
18. D. W. Peaceman and H. H. Rachford, Jr, The numerical solution of parabolic and elliptic differential equations, *J. Soc. Indust. Appl. Math.* **3,** 28–41 (1955).